

The Occurrence Rate of Nearby Planetary Companions to Hot Jupiters

LIZHOU SHA ,¹ ANDREW M. VANDERBURG ,² CHELSEA X. HUANG ,³ SAMUEL CHRISTIAN ,⁴ NICHOLAS SAUNDERS ,^{5,6}
KHALID BARKAOUI ,^{7,8,9} ALEXANDER BELINSKI ,^{10,11} SERGE BERGERON ,^{12,13} ALLYSON BIERYLA ,² KAREN A. COLLINS ,²
GIUSEPPE CONZO ,¹⁴ AKIHIKO FUKUI ,^{15,7} TRISTAN GUILLOT ,¹⁶ KAI IKUTA ,¹⁷ DAVID W. LATHAM ,² JEROME P. DE LEON ,¹⁵
BOB MASSEY ,¹³ GABRIEL MURAWSKI ,¹⁸ FELIPE MURGAS ,^{7,19} NORIO NARITA ,^{15,20,7} MOHAMMAD ODEH ,²¹ ENRIC PALLE ,^{7,19}
RICHARD P. SCHWARZ ,² GREGOR SRDOC,²² CHRIS STOCKDALE ,²³ IAN A. WAITE ,³ AND FRANCIS P. WILKIN ,²⁴

(Received October 3, 2025; Revised January 16, 2026)

Submitted to AJ

ABSTRACT

Of the > 500 confirmed transiting hot jupiters and ≈ 2000 additional candidates today, only ten are known to have nearby companion planets. The survival of nearby companions means that these hot jupiters cannot have migrated to their present location via dynamically disruptive high-eccentricity migration but instead have undergone disk migration or formed in situ. The occurrence rate for these nearby companions, therefore, constrains the relative efficiency of different hot jupiter formation pathways. Here, we perform a uniform box least-squares search for nearby transiting companions to hot jupiters in the first five years of TESS data. Accounting for observational completeness and detection efficiency, we arrive at an occurrence rate of $(7.6^{+5.5}_{-3.8})\%$, which is a lower limit on the fraction of hot jupiters that underwent disk migration or in situ formation. Comparing this rate with that derived from transit-timing variation searches suggests that hot jupiters are likely mostly aligned with their nearby companions, but their apparently higher incidence of grazing transits may point to a slight preferential misalignment. We also synthesize evidence that hot jupiters with nearby companions may have cold companions at a rate similar to that of other hot jupiters. Comprehensive transit, radial velocity, and stellar obliquity measurements in hot jupiter systems with nearby companions will be necessary to fully account for the relative prevalence of proposed hot jupiter formation pathways.

Keywords: Hot Jupiters (753); Exoplanet systems (484); Transit photometry (1709); Exoplanet migration (2205)

1. INTRODUCTION

Hot jupiters were among the first exoplanets ever discovered, yet thirty years after their initial detection (M. Mayor & D. Queloz 1995), their formation remains a mystery. Conventional theories of planet formation (e.g. J. B. Pollack et al. 1996) predicted that gas giant planets like Jupiter and Saturn should only form at large distances from their host stars where volatile materials exist in solid form (beyond the volatiles' so-called "ice lines"). The initial discovery of hot jupiters, with orbital periods less than 10 days and masses similar to or exceeding that of Jupiter, therefore came as a surprise.

In the intervening thirty years, several theories have emerged to explain the existence of these planets. A key idea in most of these explanations is that planets' orbital locations can change significantly over their lifetimes in a process called migration. This way, a gas giant planet might form in colder regions of the protoplanetary disk, and then afterwards move into much closer orbits typical of hot jupiters. There are two

main mechanisms generally believed to be responsible for hot jupiter migration: high-eccentricity (or tidal) migration (e.g. F. A. Rasio & E. B. Ford 1996), and disk migration (e.g. D. N. C. Lin et al. 1996). In high-eccentricity migration, a Jupiter-sized planet that formed beyond the ice line is perturbed into a highly eccentric orbit by gravitational interactions with an outer planetary or even stellar companion. From there, tides raised in the planet during its periastron passages gradually dissipate orbital energy and shrink the semimajor axis until the planet circularizes to a short period. On the other hand, in the disk migration scenario, the hot jupiter forms before the protoplanetary disk completely dissipates and interacts with the disk to gradually reduce its orbital period. Another possibility (although a minority opinion in the field) is that some hot jupiters may be able to form near their current orbital locations after being seeded by super-Earth-sized planets (K. Batygin et al. 2016). Understanding which of these

mechanisms are responsible for the known population of hot jupiters and in what proportions is a major goal of the field.

One way to discriminate these formation pathways is to look for smaller planets orbiting interior to hot jupiters. Because high-eccentricity migration is such a disruptive event, it is expected that no inner companion could have survived from being ejected from the system. Thus, if an inner companion is found, we could all but eliminate high-eccentricity migration as how that hot jupiter could have formed. For 20 years after the discovery of 51 Pegasi b, no hot jupiters were found to have close planetary companions (e.g. [E. Miller-Ricci et al. 2008](#); [J. H. Steffen et al. 2012](#)), even while smaller planets frequently were found in multi-planet systems ([D. W. Latham et al. 2011](#)). The apparent loneliness of hot jupiters suggested that high-eccentricity migration was likely the dominant formation pathway. However, the discovery of close planetary companions around the hot jupiter WASP-47 ([J. C. Becker et al. 2015](#)) showed that at least some hot jupiters form in a dynamically quiet manner, either via disk migration or *in-situ*. Since then, several other hot jupiter systems with close companions have been discovered ([W. Zhu et al. 2018](#); [C. I. Cañas et al. 2019](#); [C. X. Huang et al. 2020a](#); [B. J. Hord et al. 2022](#); [G. Maciejewski et al. 2023](#); [L. Sha et al. 2023](#); [J. Korth et al. 2024](#); [B. J. McKee et al. 2025](#); S. Quinn et al., in preparation, J. Livesey et al.; in preparation). Studying the population of close planetary companions to hot jupiters presents an opportunity to constrain the fraction of these systems that formed via dynamically quiet pathways. An early estimate of the occurrence rate of close companions to hot jupiters suggested these systems were indeed rare ([C. Huang et al. 2016](#)), but with only a single detected system at the time, the estimate was uncertain.

Fortunately, NASA's Transiting Exoplanet Survey Satellite (*TESS*) is enabling dramatic advancements in demographic studies of hot jupiter systems. Although hot jupiters have been routinely detected for decades, they are intrinsically rare ([J. T. Wright et al. 2012](#)) and it is difficult to construct large statistical samples. Before *TESS*, the best statistical sample of hot jupiters was that from the *Kepler* mission, but because *Kepler* was only able to downlink data for about 200,000 stars, it only detected 40–60 hot jupiters from its primary mission ([S. E. Thompson et al. 2018a](#); [S. W. Yee et al. 2021](#)). *TESS*, on the other hand, observes and downlinks data for millions of stars bright enough for hot jupiter detection each month. As a result, it has already observed thousands of hot jupiters ([N. M. Guerrero et al. 2021](#)), the vast majority of which are new discoveries (e.g. [S. W. Yee et al. 2022, 2023](#); [J. E. Rodriguez et al. 2021, 2023](#); [J. Schulte et al. 2024](#)). This large number of discoveries, coupled with *TESS*'s very high sensitivity to these planets (making large magnitude and volume-limited samples nearly complete) and relatively unbiased target selection, have enabled important advancements in hot jupiter

population studies (e.g. [G. Zhou et al. 2019](#); [M. Beleznay & M. Kunimoto 2022](#); [S. W. Yee & J. N. Winn 2023](#)). Among these results is the first measurement of the occurrence rate of close companions around hot jupiters by [B. J. Hord et al. \(2021\)](#), who used a sample of about 179 hot jupiters to determine that about $7.3_{-7.3}^{+15.2}\%$ of hot jupiters have a close planetary companion – the first constraint on the fraction of hot jupiter systems that must form in a dynamically quiet manner. However, the relatively large uncertainty on the occurrence rate (a consequence of the relatively small number of hot jupiters searched), limits the strength of conclusions about hot jupiter formation that can be drawn.

In this work, we perform the largest ever uniform search for transiting inner companions to transiting hot jupiters in *TESS* data. We identify around two thousand likely hot jupiters from the *TESS* planet candidate catalog and search their light curves for close transiting companions. We carefully vet any new signal and eliminate known astrophysical false positives such as eclipsing binaries or stellar variations. We characterize the sensitivity of our pipeline and calculate a refined occurrence rate for close companions, given the existence of these hot jupiters. Our paper is organized as follows: Section 2 describes our sample selection, Section 3 discusses our planet search pipeline, and we list the detected signals in Section 4. We describe the methodology behind our occurrence rate calculations and their results in Section 5, and we discuss the implications of these measurements in Section 6 before concluding in Section 7.

2. SAMPLE OF HOT JUPITERS

We aimed to search every hot jupiter observed during the first five years (sectors 1–69) of the *TESS* mission for nearby planetary companions ($P < 10$ d). To that end, we assembled a list of confirmed and candidate hot jupiters from the *TESS* Objects of Interest (TOI; [N. M. Guerrero et al. 2021](#)) Catalog. After carefully removing known or suspected non-planets, we estimated the false positive rate (FPR) of the remaining planet candidates on our list. Finally, we derived new stellar parameters from broadband photometry as the basis for refined planetary parameters of the hot jupiters. These procedures are detailed in the rest of this section.

2.1. Selecting hot jupiters

To start, we select TOI candidates

1. with valid *Gaia* DR2 cross-matches,
2. periods $P < 10$ d,
3. radii $8 \leq R_p/R_\oplus < 30$ within uncertainty and measured to better than 50%, and
4. alerted on or before UT 2024 May 30

Table 1. Hot jupiter candidates from the *TESS* Objects of Interest (TOI) catalog.

TIC ID	Period d	Mid-transit time BJD _{TDB} – 2,457,000	Transit depth	Duration h	Stellar mass M _⊙	Stellar radius R _⊙	Planet radius R _⊕	<i>a/R</i> _★	Impact param.
4711	2.33481520	2358.079233	0.005310	1.86	1.202	1.432	11.4	5.499	0.912
56884	3.91748200	3088.668722	0.008397	2.62	1.322	1.574	15.7	7.292	0.890
160023	6.75655190	2358.443291	0.005200	3.44	1.214	1.622	12.8	9.893	0.847
857186	3.81236140	2465.891746	0.018330	2.56	0.826	0.788	11.6	12.227	0.365
1003831	1.65114558	1518.203428	0.003206	0.95	1.008	1.077	6.7	5.472	0.976
1129033	1.36002828	2168.520849	0.019428	2.17	0.982	1.045	15.9	4.913	0.526
...

NOTE—The first five columns are taken from the TOI Catalog (N. M. Guerrero et al. 2021, accessed on 2024 July 5). The stellar masses and radii are from this work, and the last three columns are imputed from the values in the preceding columns assuming circular orbits (subsection 2.3). These parameters are used in section 5 to calculate observational completeness. While the values in this table are self-consistent and valid in the statistical aggregate, they should not be used in work demanding high accuracy in the context of individual planetary systems. (This table is available in its entirety in machine-readable form in the online article.).

from the ExoFOP website (NExSci 2022, accessed on 2024 July 5). To identify TOI candidates that are known or suspected to not be planets, we eliminated targets with

1. unfavorable dispositions of the *TESS* Follow Up Program working group (TFOPWG)²⁵ from the ExoFOP website (accessed on 2025 March 11), and
2. excess radial velocity (RV) scatter from *Gaia* DR3, and
3. $R_p \geq 30 R_\oplus$ and semimajor axis-to-stellar radius ratio $a/R_\star < 1$ based on the parameters derived in subsection 2.3.

The TFOPWG dispositions are based on follow-up photometry, spectroscopy, and high-resolution imaging and identify TOI candidates that are known or suspected to be eclipsing binaries or other astrophysical false positives. The RV scatters from *Gaia* DR3 eliminate suspected spectroscopic binaries. We estimate the RV scatter σ_{RV} by multiplying the reported RV uncertainty (`radial_velocity_error`) and the square root of the number of RV observations (`rv_nb_transits`). Then, we use the following empirical formula based on *Gaia* DR3 *G* magnitude to identify the targets with excess σ_{RV} :

$$\frac{\sigma_{\text{RV}}}{\text{km s}^{-1}} > \begin{cases} 2 & G < 10, \\ 2 \cdot 10^{0.4(G-10)} & G \geq 10. \end{cases} \quad (1)$$

The TOI candidates that survive these checks comprise our sample of hot jupiters searched for nearby companions, as long as their *TESS* light curve is available. They are tabulated in Table 1.

²⁵ Specifically, we eliminated planets designated as false positive (FP), false alert (FA), and ambiguous planetary candidates (APC) by the TFOPWG.

2.2. Estimation of false positive rate

In order to ensure the accuracy of our calculated occurrence rate (subsection 5.4), we want to estimate the FPR, defined as the fraction of non-planets, in our hot jupiter sample. Starting from the original estimate for the FPR of TOIs from G. Zhou et al. (2019) based on 10 detected false positives among 31 TOIs, which we denote $\text{FPR}_{\text{Zhou}} = 10/31 \approx 0.32$, we expect to find $\text{FPR}_{\text{Zhou}} \cdot N_{\text{TOI}}$ false positives among the $N_{\text{TOI}} = 2684$ TOIs that match our initial period, radius, and alert time criteria. We subsequently eliminated 570 confirmed or suspected non-planets based on TFOPWG dispositions, 249 suspected spectroscopic binaries based on excess σ_{RV} , and 16 suspected non-planets with implausible R_p or a/R_\star for a combined total of $N_{\text{FP}} = 749$. In theory, this elimination leaves us with

$$\text{FPR}_{\text{HJ}} = \frac{\text{FPR}_{\text{Zhou}} \cdot N_{\text{TOI}} - N_{\text{FP}}}{N_{\text{TOI}} - N_{\text{FP}}} \approx 0.060 \quad (2)$$

among the remaining 1935 hot jupiters in our sample. This FPR_{HJ} will be used in subsection 5.4 to adjust the final effective sample size of the hot jupiters for the occurrence rate calculation.

2.3. Properties of the hot jupiters and their host stars

In order to obtain more accurate planetary parameters, we derived mass and radii for the hot jupiter host stars via spectral energy distribution (SED) fitting to *Gaia* DR3 *G*, *G_{BP}*, *G_{RP}* magnitudes and 2MASS *J*, *H*, *K* magnitudes. We obtained these magnitudes by cross-matching the *TESS* Input Catalog version 8 (TICv8; K. G. Stassun et al. 2018, 2019) with the *Gaia* and 2MASS catalogs. (The targets that did not have *Gaia* DR2 cross-matches in TICv8 were not selected in the first place.) Given these broadband apparent magnitudes, and *Gaia* DR3 parallaxes, we used the ISOCHRONES Python package (T. D. Morton 2015) to perform nested sampling of fundamental stellar parameters modeled by the MESA Isochrones

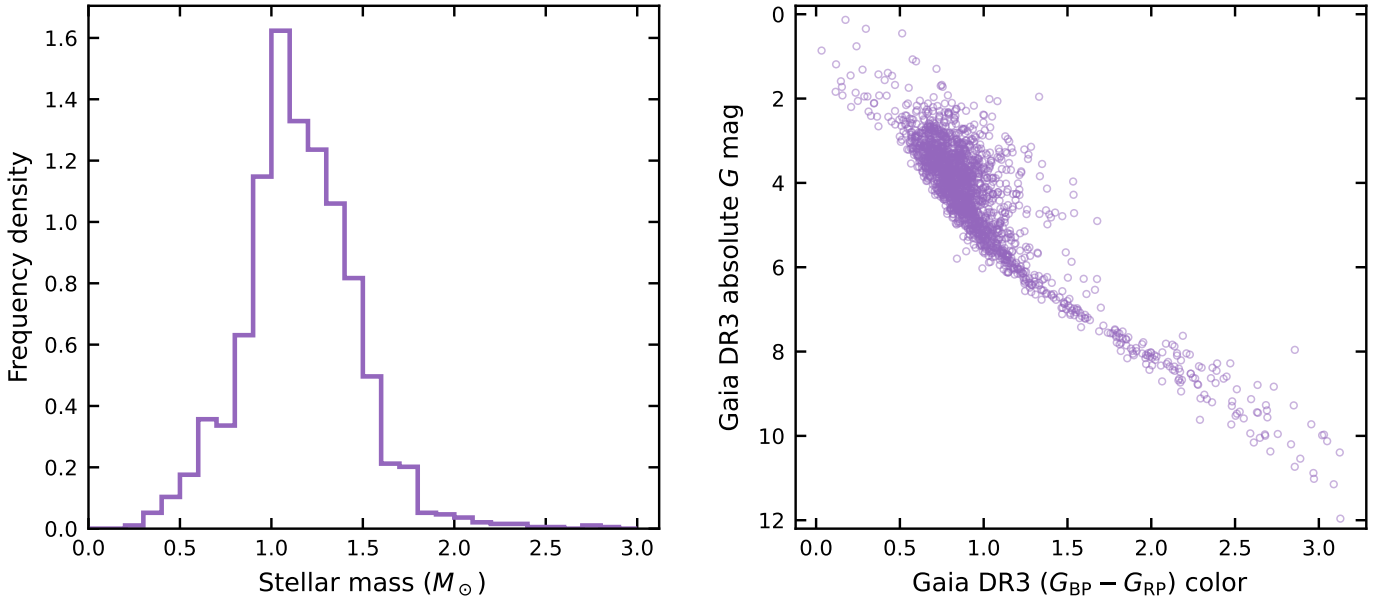


Figure 1. The distribution of the host stars of the selected hot jupiters. *Left:* The histogram of stellar mass. *Right:* The color–magnitude diagram.

and Stellar Tracks (MIST; [A. Dotter 2016](#); [J. Choi et al. 2016](#)), using the associated correction tables to convert bolometric to broadband photometric magnitudes. To better reflect systematic and model uncertainty, we inflated the uncertainty for all measured magnitudes to 0.1.

The resulting new stellar masses M_\star and radii R_\star , as well as derived planetary parameters, are tabulated in [Table 1](#), and the distribution of stellar masses and the color–magnitude diagram are shown in [Figure 1](#). We derived planet radii R_p from the new R_\star and the transit depth from the TOI catalog and used the new M_\star and R_\star combined with the orbital period from the TOI catalog to calculate a/R_\star , which is then used in conjunction with our derived R_p and the transit duration from the TOI catalog to calculate the impact parameter b , assuming circular orbits. As mentioned in [subsection 2.1](#), we further identified all planets with $R_p \geq 30 R_\oplus$ and $a/R_\star < 1$ and eliminated them from the hot jupiter sample as likely non-planets. Since TOIs must be transiting, we clamp this derived b to the interval $[0, 1 + R_p/R_\star]$. These new M_\star , R_\star and derived R_p , b will be used to determine observational completeness for the occurrence rate calculation in [section 5](#).

3. SEARCH FOR ADDITIONAL SHORT-PERIOD PLANETS IN HOT JUPITER SYSTEMS

To search for nearby transiting companions of hot jupiters, we used light curves from the MIT Quick Look Pipeline (QLP) up to and including sector 69. Initially created for the *TESS* Prime Mission, QLP generates light curves for all targets in the *TESS* full-frame images (calibrated as described by [M. M. Fausnaugh et al. 2020](#)) brighter than a *TESS* magnitude of 13.5 and certain fainter targets with high proper motion ([C. X. Huang et al. 2020b,c](#); [M. Kunimoto et al. 2021](#),

[2022b](#)). Since we perform detrending, or removal of the long-term variability in the light curves, as part of the planet search, we use the raw simple aperture photometry (SAP_FLUX) time series for light curves before sector 56 and the systematics-corrected (SYS_RM_FLUX) time series thereafter ([M. Kunimoto et al. 2022a](#)). There were 86 targets out of the 1935 hot jupiter systems in our sample without valid QLP light curves, leaving us with $N_{\text{HJ}} = 1849$ systems to be searched. We detail our planet search pipeline and candidate vetting procedures in this section.

3.1. Box least-squares search

We used the box least squares (BLS; [Kovács, Zucker, & Mazeh 2002](#)) algorithm to search for additional planets in the light curves of the hot jupiters. After removing all points that have been flagged for quality issues (e.g. spacecraft anomaly, excess scattered light, etc.), we iteratively applied the following steps five times to each light curve:

1. Remove parts of the light curve containing hot jupiter transits and signals corresponding to the previous peaks of the light curve.
2. Detrend the light curve, remove upward outliers, and estimate uncertainty.
3. Find the period and phase of the signal corresponding to the peak of the BLS power spectrum.

We detail these steps below.

Removal of known signals—We remove the hot jupiter transits from the raw photometry light curve by masking points that lie within a span of three times the transit duration centered

on the mid-transit time, with the transit ephemerides taken from the TOI Catalog. In subsequent iterations, we also remove portions of the light curve corresponding to signals detected in previous iterations.

Detrending—We detrend the light curves using Keplerspline, a high-pass filtering method based on B-spline (A. Vanderburg & J. A. Johnson 2014; C. J. Shallue & A. Vanderburg 2018)), in segments that are no more than approximately 14 days and also contain no gaps longer than 1 day. Keplerspline uses the Bayesian information criterion to automatically pick the most appropriate breakpoint spacing for each light curve. The detrended segments are then normalized and joined together to search for additional planets. Keplerspline estimates the standard deviation σ of the light curve from the median absolute deviation. This σ is calculated per sector and is used as the nominal uncertainty for all data points in a given sector for the subsequent transit search. We also reject points that lie more than 5σ above the spline in order to mitigate the effect of flares and instrumental artifacts on the transit detection algorithm.

Performing the BLS search—We use the CUVARBASE (J. Hoffman 2022) package for BLS search, similar to QLP’s implementation since sector 59 (M. Kunimoto et al. 2023). The CUVARBASE package uses the NVIDIA CUDA interface to implement BLS on the GPU. We search in the period range of 4 hours to 10 days with the optimal frequency spacing $\delta f \propto f^{2/3}$ and a log-uniform grid of the transit duration fraction with 20 intervals between 2^{-7} and 2^{-2} . Since we use a fast implementation of BLS that only outputs the BLS power at each period, once we obtain the period with the highest BLS power, we use the ASTROPY package to obtain the transit parameters (mid-transit time, transit duration T_{dur} , and depth δ) at the detected period, following the methods implemented by VARTOOLS (J. D. Hartman & G. A. Bakos 2016). These parameters are used in subsequent iterations for signal removal.

3.2. Vetting transit-like signals

We declared any signal with a BLS signal-to-noise ratio $S/N > 7$ as computed by ASTROPY to be a threshold-crossing event (TCE), and all TCEs are vetted to ensure they are likely to be transiting planets. We applied the following criteria in order to automatically eliminate TCEs of low data quality or whose parameters are incompatible with being a planet:

1. number of points in transit ≥ 20 ,
2. number of transits (each with ≥ 3 points) ≥ 3 ,
3. $a/R_{\star} > 3$, where a is the semimajor axis and R_{\star} is the stellar radius, and
4. $T_{\text{dur}} < 3 T_{\text{dur,circ}}$, the transit duration assuming a circular orbit and impact parameter $b = 0$.

Both a/R_{\star} and $T_{\text{dur,circ}}$ were calculated from the stellar masses and radii from TICv8 and the period and transit depth of the TCE. All TCEs that fulfill these criteria, as well as TCEs whose stellar parameters are missing from TICv8, were retained for manual vetting.

We performed manual vetting in two distinct steps. In the first step, we generated three types plots for each TCE: the BLS spectrum, the folded light curve centered on the TCE with binned points and the boxcar transit model, and undetrended light curves with the detrending spline and the transit signals highlighted. We used these plots to eliminate TCEs that

1. were not transit-like in shape,
2. showed significant odd–even variations, or
3. could be attributed to fast varying portions of the light curve (e.g. scattered light near the beginning or end of an orbit) that the detrending step did not remove.

TCEs that survived the initial manual vetting were subject to additional scrutiny. We generated additional light curves with enhanced systematics correction from the full frame images by extracting aperture photometry following A. Vanderburg et al. (2016) and correcting for spacecraft systematics using the procedures described by A. Vanderburg et al. (2019). These additional light curves were used to generate additional vetting plots, including a cutout view of the *TESS* FFI and a simple pixel-level difference image of the median in- and out-of-transit FFIs, with a customized version of the GIANTS package²⁶ (N. Saunders et al. 2022). Since *TESS* has a relatively large pixel size of $21''$, the photometric aperture could enclose nearby targets that are blended or unresolved from the true target. Therefore, we also eliminated TCEs that showed a significant offset in the in- and out-of-transit difference image from the expected centroid of the target star. For the few TCEs that passed all previous vetting steps but were not known confirmed or candidate planets, we further used the TRANSIT-DIFFIMAGE package²⁷ by S. Bryson to calculate accurate centroids of the TCE and the assumed host star taking account of the pixel response function (PRF).

Finally, we eliminated secondary eclipses by matching them to the period and epoch of the star. We used the expected depth of the secondary eclipse as well as the phase offset from the known hot jupiter transits and we manually inspected each light curve to rule out that they could be planets at half or twice the hot jupiter’s orbital period.

²⁶ The original version is available on GitHub at <https://github.com/nksaunders/giants>.

²⁷ Available on GitHub at <https://github.com/stevepur/transit-diffImage>.

The TCEs that passed all above vetting steps are the planet detections listed in section 4. These detections are used as the numerator of the occurrence rate in section 5.

3.3. Injection–recovery simulation

In order to evaluate the detection efficiency of the planet search pipeline described in subsection 3.1 and the vetting procedures described in subsection 3.2, we performed injection–recovery tests of simulated transit signals. For each host star in the hot jupiter sample, five simulated signals were created via randomly drawn planetary parameters from the prior distributions

$$R_p \sim \mathcal{U}(0.5, 10) R_\oplus, \quad (3a)$$

$$\log P \sim \mathcal{U}(4 \text{ h}, 10 \text{ d}), \quad (3b)$$

$$b \sim \mathcal{U}(0, 1 + R_p/R_\star), \quad (3c)$$

with stellar mass and radius from TICv8 when available or fixed to Solar values otherwise.²⁸ All orbits were assumed to be circular, and we adopted a fixed linear limb darkening law with coefficient 0.3. We calculated the simulated signals from these parameters using the limb-darkened transit light curve model implemented by the BATMAN Python package, and the model was supersampled by a factor of 15, 5, and 2 for *TESS* sectors with FFI exposure times 30 min, 10 min, and 200 s, respectively. Each simulated signal was injected into the corresponding hot jupiter host star’s *TESS* light curve, and we searched the resultant light curve using the same BLS transit search pipeline as in subsection 3.1. As before, we used $S/N > 7$ as the criterion for declaring a BLS signal to be a TCE.

Rather than manually vetting the TCEs as in subsection 3.2, we automatically matched the detected TCEs to the expected period and transit times using the ephemeris matching method described by J. L. Coughlin et al. (2014). Using their definition, we set the criteria for ephemeris-matching to be

$$\sigma_P > 3.5, \quad \sigma_T > 2.0, \quad (4)$$

where P is the period and T is the transit time or epoch and the σ values are converted from the fractional differences in P or T (J. L. Coughlin et al. 2014). Figure 2, emulating Figure 2 by J. L. Coughlin et al. (2014), confirms that the chosen significance levels in Equation (4) capture the mode of true ephemeris matches in the upper right while excluding

²⁸ Since the injection–recovery simulation is only used to derive an empirical relationship between theoretical transit S/N and pipeline detection efficiency, the exact choice of stellar parameters here has no bearing on the final occurrence rate as long as the range of S/N is sufficiently sampled. Rather, the choice of stellar parameters affects the final result through the assumed planet radius prior distribution in Equation (12b), where we did use the refined stellar parameters from subsection 2.3 to derive the imputed transit depth of each simulated planet.

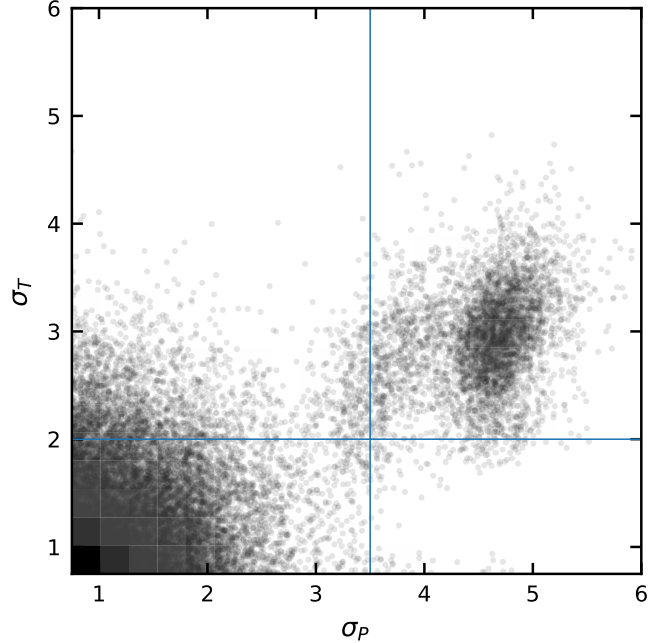


Figure 2. A scatter plot of σ_P versus σ_T for the detection of injected transit signals, similar to Figure 2 by J. L. Coughlin et al. (2014). The thin blue lines denote the chosen significance levels for ephemeris matching in equation (4) and divides the plane into four quadrants. The cluster of points in the upper right quadrant corresponds to true ephemeris matches, while the cluster of points in the lower left are random false matches.

the mode of random matches at low σ_P and σ_T values in the lower left. The number of matches as a fraction of injected signals is the empirical detection efficiency, which we denote ϵ , and we evaluate its dependence on the transit S/N in subsection 3.4.

3.4. Transit detection efficiency

The injection–recovery simulation resulted in a map of sets of simulated planetary parameters to Boolean values indicating success or failure of recovery. For the convenience of calculating the occurrence rate later in section 5, we convert the injection–recovery results into an analytical formula that expresses the fraction of planets successfully detected by our search in terms of their transit signal’s theoretical S/N.

We calculate a planet’s theoretical transit S/N as

$$S/N = \frac{\delta}{\sqrt{\sigma_{\text{sum}}^2 P/T_{\text{dur}}}}, \quad (5)$$

where δ is the transit depth, P is the orbital period, T_{dur} is the transit duration, and σ_{sum}^2 is the “harmonic sum” of σ_i^2 , the squared uncertainty of the i th data point ($i = 1, 2, \dots, N$)

$$\sigma_{\text{sum}}^2 = \left(\sum_{i=1}^N \frac{1}{\sigma_i^2} \right)^{-1}. \quad (6)$$

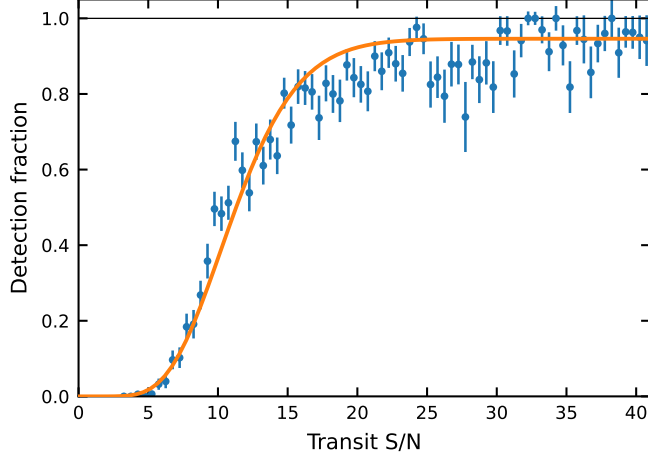


Figure 3. Detection fraction as a function of transit S/N. The blue marks are the recovery fraction of injected planets within each S/N bin with error bars representing the Agresti–Coull confidence interval of binomial proportion, and the orange curve is a scaled gamma distribution CDF. The detection fraction asymptotically approaches ≈ 0.95 as the transit S/N $\rightarrow \infty$.

In the case that the data points have identical σ_i , this expression reduces to the familiar $\sigma_{\text{sum}}^2 = \sigma_i^2/N$.

In order to relate the theoretical S/N to the actual detection fraction, we empirically fitted the cumulative distribution function (CDF) of the gamma distribution with a shape parameter α , scale parameter θ , and maximum detection fraction C :

$$F(x; \alpha, \theta, C) = \frac{C}{\Gamma(\alpha) \theta^\alpha} \int_0^x t^{\alpha-1} e^{-t/\theta} dt, \quad (7)$$

as was used by (J. L. Christiansen et al. 2015) for characterizing the transit signal recovery of the *Kepler* pipeline. To properly account for the statistics of the binned detection fraction, we used the Agresti–Coull interval (A. Agresti & B. Coull 1998) where the number of trials n and the success fraction p are modified into their estimators

$$\hat{n} = n + 1, \quad \hat{p} = \frac{1}{\hat{n}} \left(p + \frac{1}{2} \right), \quad (8)$$

which are used to calculate the interval

$$\sqrt{\frac{\hat{p}(1 - \hat{p})}{\hat{n}}}. \quad (9)$$

We used the unmodified p for each S/N bin and the Agresti–Coull interval as the uncertainty in each bin.

We ended up with the best-fit parameters

$$\alpha = 9.21719769, \theta = 1.24222051, C = 0.94609528, \quad (10)$$

given to 8 decimal places (understood as machine precision and not as significant figures). This scaled gamma CDF $F(x)$, illustrated in Figure 3, will be used in section 5 to convert the theoretical transit S/N of the simulated planets into the expected pipeline detection efficiency ϵ by setting $x = \text{S/N}$.

4. PLANET DETECTIONS

We detected the following inner companions, in ascending order of the orbital period of their respective hot jupiters:

1. TOI-1408 c (J. Korth et al. 2024),
2. TOI-5143.02 (S. Quinn et al., in preparation),
3. TOI-1130 b (C. X. Huang et al. 2020a),
4. TOI-2494.02 (S. Quinn et al., in preparation),
5. WASP-84 c (G. Maciejewski et al. 2023), and
6. TOI-2000 b (L. Sha et al. 2023).

Of these, TOI-2000 b was discovered by an earlier version of the pipeline described in subsection 3.1. These detections form the basis of the occurrence rate calculation in section 5.

The following known nearby companions were not among those detected:

1. WASP-47 e and WASP-47 d, the inner and outer companions to WASP-47 b,
2. TOI-4468.02, the outer companion to TOI-4468.01 (J. Livesey et al., in preparation),
3. Kepler-730 c, the inner companion to Kepler-730 b, and
4. WASP-132 c, the inner companion to WASP-132 b.

The hot jupiters WASP-47 b and TOI-4468.01 were included in our sample, but their respective companions were not detected by the pipeline. The hot jupiter Kepler-730 b was not a TOI and thus not in the sample. The hot jupiter WASP-132 b was not in the sample because it lacked uncertainty for its radius in the TOI table on the ExoFOP website at the time of access. They will not count as detections for the purpose of the occurrence rate calculation.

Figure 4 presents a “family portrait” visualization of the architectures of these ten systems.

5. OCCURRENCE RATE OF NEARBY COMPANIONS TO HOT JUPITERS

Our goal is to estimate the occurrence rate η of nearby companions to hot jupiters, conditioned on the hot jupiter existing. To this end, we use a Bayesian statistical framework to calculate the posterior distribution of η given our sample of transiting companions to transiting hot jupiters from *TESS*. We model each hot jupiter observation as a Bernoulli trial where the probability of success is η . Then, given n such conditionally independent Bernoulli trials with s observed successes and a uniform prior for η , the posterior distribution of η can be modeled as the beta distribution $\text{Beta}(s + 1, n - s + 1)$,

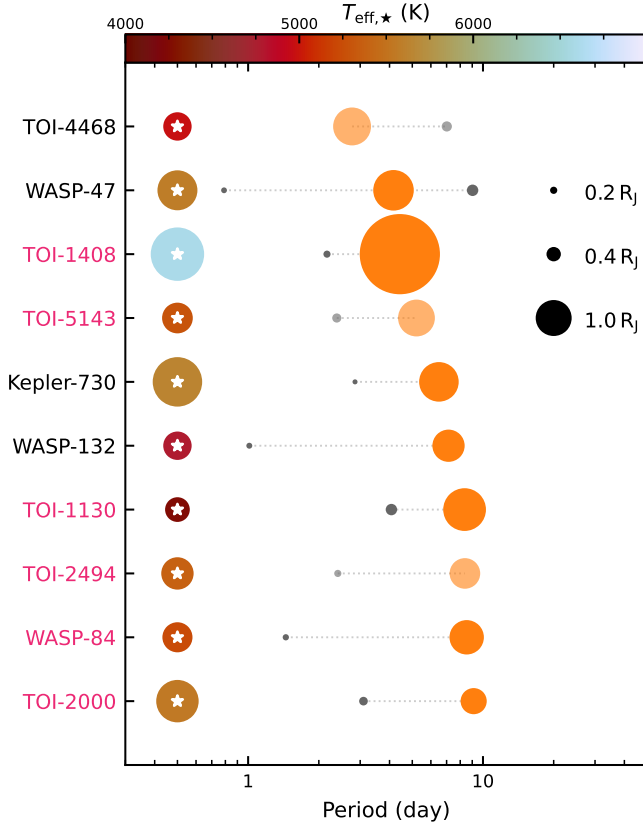


Figure 4. Transiting planetary systems hosting nearby planetary companions to hot Jupiters ($P < 10$ d). Non-transiting planets are omitted. The leftmost circle in each row represent the host star, with the mark's size indicating the stellar radius and fill color the stellar effective temperature (from TICv8; K. G. Stassun et al. 2019). The other circles represent the transiting planets in each system, with their sizes proportional to planet radii and fill colors indicating a giant planet (orange) or a small planet (gray). The relative mark sizes among either the stars or the planets are to scale, but not between a star and its planets. The translucent marks are planet candidates not yet published in the literature. Systems which are counted as detected (section 4) for the occurrence rate calculation (section 5) have their names highlighted in magenta. The systems are sorted in ascending order of the period of the largest planet. This figure and its caption are adapted from Figure 10 by L. Sha et al. (2023).

which is the conjugate prior of the binomial distribution. The PDF of η can be written as

$$f(\eta; s, n) = \frac{\eta^s (1 - \eta)^{n-s}}{B(s+1, n-s+1)}, \quad (11)$$

where B is the beta function. We take $s = 6$ as the number of hot Jupiters with detected companions (section 4), while the number of trials n is the number of hot Jupiter systems searched corrected for observational completeness and accounting for the possibility of hot Jupiter false positives.

Observational completeness concerns two questions regarding a hypothetical companion to an hot Jupiter. First, given the orbital and planet parameters, does the companion

transit? Second, if the companion transits, how likely is its detection? In order to evaluate these two questions for each hot Jupiter system, we simulated 10,000 hypothetical companions with the following procedure.

1. The companion's radius, orbital period, and mutual inclination with the hot Jupiter is drawn from a prior distribution.
2. The companion's impact parameter is calculated from the mutual inclination and the inclination of the hot Jupiter.
3. If the impact parameter indicates that the companion does not transit, the detection efficiency ϵ is set to zero, and we move on to the next simulated planet. Otherwise, we calculate the expected transit S/N and convert it into a predicted efficiency as $\epsilon = F(S/N)$, with F being the empirically derived gamma CDF in subsection 3.4.

Finally, we sum up the average detection efficiency of the simulated companions in each hot Jupiter system to arrive at an effective sample size (ESS) of the hot Jupiters searched, which we take to be the number of trials n . The rest of this section describes each step in detail.

5.1. Prior distribution of nearby companions

We draw the companion's radius R_p , orbital period P , and mutual inclination ψ from the following distributions:

$$R_p \sim \mathcal{U}(1, 4) R_\oplus, \quad (12a)$$

$$P \sim \mathcal{U}(0.25, 10) \text{ d}, \quad (12b)$$

$$\psi \sim \text{Rayleigh}(1.8), \quad (12c)$$

where $\mathcal{U}(a, b)$ is the uniform distribution on the interval $[a, b]$ and Rayleigh(σ) is the Rayleigh distribution with the scale parameter σ , subject to the condition

$$a/R_\star > 2. \quad (13)$$

For ease of comparison, we follow C. Huang et al. (2016) in setting σ to 1.8 (in radians), a value which was in turn based on an estimate of 1.0 – 2.2 for ψ in *Kepler* multi-transiting systems by D. C. Fabrycky et al. (2014). We will explore how the inferred occurrence rate changes with the choice of prior distributions for ψ in subsection 5.5.

5.2. Mutual inclination and impact parameter

We calculate the impact parameter of the simulated companion from its ψ in order to find its transit duration, on which the transit S/N depends. We sampled the companion's inclination i_2 through the relation

$$\cos i_2 = \cos i_1 \cos \psi + \cos B \sin i_1 \sin \psi, \quad (14)$$

where i_1 is the inclination of the hot jupiter derived from its impact parameter (derived in subsection 2.3) and B is an angle randomly drawn from $\mathcal{U}(0, 360^\circ)$.²⁹ The companion's impact parameter b_2 is then calculated from $\cos i_2$ assuming a circular orbit.

If $b_2 > 1 + R_p/R_\star$, the planet is deemed not transiting, and its detection efficiency is set to zero. Otherwise, we proceed to calculate its transit S/N and detection efficiency as in subsection 3.4 using the stellar radii from subsection 2.3.

5.3. Observational completeness and effective sample size

To calculate an effective sample size (ESS), we sum up the average detection efficiency ε of the simulated companions in each hot jupiter system. In mathematical notation, the total ESS is

$$\text{ESS} = \sum_{j=1}^{N_{\text{HJ}}} \frac{1}{N_{\text{sim}}} \sum_{i=1}^{N_{\text{sim}}} \varepsilon_{ij}, \quad (15)$$

where ε_{ij} is the detection efficiency of the j th simulated companion of the i th hot jupiter, $N_{\text{sim}} = 10,000$ is the number of simulated companions per each hot jupiter, and N_{HJ} is the number of hot jupiter systems in our sample. Figure 5 shows the average ε_{ij} in bins of planet period and radius expressed as percentages. Note that $\varepsilon_{ij} \equiv 0$ for non-transiting simulated companions, so the ESS is a measure of observational completeness taking account of both transit probability and pipeline detection efficiency.

Some of the hot jupiter candidates in our sample from *TESS* surveys may still be false positives (e.g. background eclipsing binaries, hierarchical triples, blended foreground binaries). We multiply the above $\text{ESS} = 92.50$ by $(1 - \text{FPR}_{\text{HJ}})$ from subsection 2.2 to obtain the final $n = 86.95$, which is substituted into equation (11) to obtain the posterior distribution PDF $f(\eta)$.

5.4. The occurrence rate

The PDF of the posterior distribution $f(\eta)$ of the occurrence rate η of nearby companions to hot jupiters is shown in Figure 6. We quote the median and 90% credible interval of the occurrence rate as $(7.6^{+5.5}_{-3.8})\%$.

5.5. Dependence on mutual inclination

In order to test the effect of orbital alignment between the hot jupiter and its nearby companion on the occurrence rate, we replace the Rayleigh distribution used in subsection 5.1 with a series of 3D von Mises–Fisher (VMF) distribution of varying parameters. The 3D VMF distribution is the analog to the 2D normal distribution on the sphere, with a PDF over

the unit vector $\hat{\mathbf{h}}$

$$f(\hat{\mathbf{h}}; \hat{\mathbf{n}}, \kappa) = \frac{\kappa}{4\pi \sinh \kappa} \exp\left(\kappa \hat{\mathbf{n}} \cdot \hat{\mathbf{h}}\right), \quad (16)$$

with $\hat{\mathbf{n}}$ being a unit vector representing the reference direction and κ a scale parameter characterizing the spread of the distribution. As such, if we take $\hat{\mathbf{n}}$ and $\hat{\mathbf{h}}$ to be the orbit normal vector of the hot jupiter and its nearby companion, respectively, then the VMF distribution is a good candidate for parameterizing their degree of alignment via the scale parameter κ . If we marginalize this distribution over the mutual inclination ψ (i.e. $\cos \psi = \hat{\mathbf{n}} \cdot \hat{\mathbf{h}}$), then we obtain the Fisher distribution with a PDF of

$$f(\psi; \kappa) = \frac{\kappa}{2 \sinh \kappa} e^{\kappa \cos \psi} \sin \psi, \quad (17)$$

which is the form often used in theoretical treatments of orbital alignment in multiplanet systems (e.g. J. C. Becker et al. 2017; D. C. Fabrycky & J. N. Winn 2009). The Fisher distribution with scale parameter κ reduces to Rayleigh($1/\sqrt{\kappa}$) for large κ and small ψ and to an isotropic distribution (i.e. uniform in $\cos \psi$) as $\kappa \rightarrow 0$, representing the cases of well-alignment versus maximal misalignment, respectively.

We find that as $\kappa \rightarrow 0$, we have $n \approx 17$ and as $\kappa \rightarrow \infty$, $n \approx 89$. This translates to an occurrence rate of $(37^{+19}_{-17})\%$ if the companion is isotropically distributed and $(7.4^{+5.4}_{-3.7})\%$ if the companion is aligned.

6. DISCUSSION

In this work, we measure the occurrence rate of close companions to hot jupiters to be $(7.6^{+5.5}_{-3.8})\%$. In agreement with previous estimates of the occurrence rates of nearby companions (C. Huang et al. 2016; B. J. Hord et al. 2021), we find that hot jupiters tend to be solitary. Historically, this fact has been taken as evidence that hot jupiter formation is dynamically violent and tends to destabilize nearby planetary companions. In this section, we revisit these conclusions in light of our new results.

6.1. Comparison to inner companions of small short-period planets

Do hot jupiters have fewer nearby companions than the typical small, short-period transiting planet, such as the ones observed by *Kepler*? Answering this question puts the loneliness of hot jupiters into the broader context of planetary system architectures. Using data from *Kepler* DR25 (S. E. Thompson et al. 2018b), we calculated the probability of a planetary system hosting small transiting short-period planets also hosting another transiting small planet nearby ($P < 10$ d). Specifically, we selected small planets with

²⁹ If we set the orbital normal vector of the hot jupiter as the z -axis, then ψ and B are respectively the polar and azimuthal angles of the companion's orbital normal vector.

1. host star effective temperatures $T_{\text{eff},\star} < 4500$ K,
2. radii $R_p < 4 R_\oplus$ (assuming *Gaia* DR2 stellar parameters),

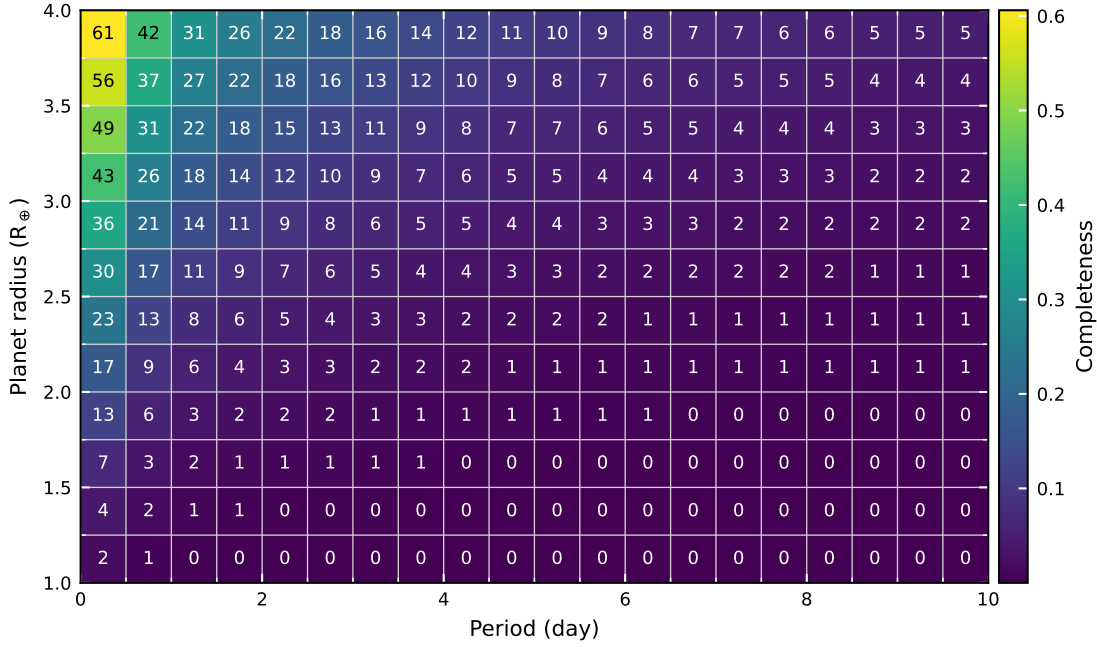


Figure 5. Overall observational completeness of simulated nearby companions to hot Jupiters in bins of the orbital periods and planet radii of the companions (subsection 5.3), expressed as percentages. The observational completeness takes account of both transit probability and detection efficiency.

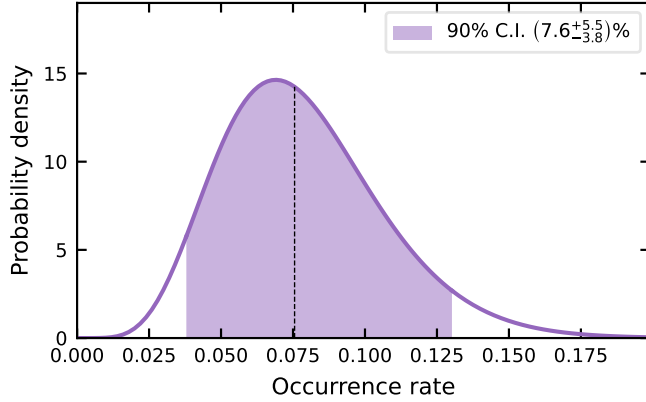


Figure 6. Posterior distribution of the occurrence rate of nearby companions ($0.25 \text{ d} \leq P < 10 \text{ d}$, $1 \leq R_p/R_\oplus < 4$) to hot Jupiters. The 90% credible interval about the median is $(7.6^{+5.5}_{-3.8})\%$, with the median indicated by a solid vertical line and the interval shaded.

3. periods $0.25 \text{ d} \leq P < 10 \text{ d}$, and
4. impact parameters $b < 0.9$.

We set an additional stellar effective temperature criterion to make sure the overall stellar sample is similar to that of hot Jupiter hosts. We found this probability is 17.5% for the small planets even without correcting for completeness, much higher than the intrinsic occurrence rate for nearby companions to hot Jupiters.

We further estimated a preliminary intrinsic occurrence rate of these inner companions using the same prior distribution of planetary parameters for the companions of hot

Jupiters described in subsection 5.1. Combined with the detection completeness functions provided by the *Kepler* team (C. J. Burke et al. 2015; J. L. Christiansen et al. 2015), we find that, on average, the probability of a system hosting a short-period small planet also host another small planet within 10 days is $(77 \pm 5)\%$. We caution that these results are highly sensitive to the choice of prior distributions for the companion’s period and radius, which is not taken into account in the uncertainties, although it would not change the conclusion that the probability having a companion is significantly higher for small short-period planets compared to hot Jupiters.

6.2. Comparing to occurrence rate obtained from transit-timing variation

Another important clue we can glean from our analysis is a constraint on the mutual inclination distribution for hot Jupiters and their close companions. The mutual inclination between an hot Jupiter and its nearby companion tells us a great deal about the formation and migration history of these systems. If the hot Jupiter and its nearby companion is well-aligned, then it is evidence that the system had a relatively quiescent dynamical history. While we can directly constrain the sky-projected orbital orientation of the hot Jupiter through Rossiter–McLaughlin measurements (R. A. Rossiter 1924; D. B. McLaughlin 1924), it is challenging to achieve the S/N required for the small companion within its transit duration. Thus, we are unlikely to directly constrain the mutual inclination between the hot Jupiter and its nearby companion in the near future. The assumed mutual inclination distribution directly affects the occurrence rate we measure by altering

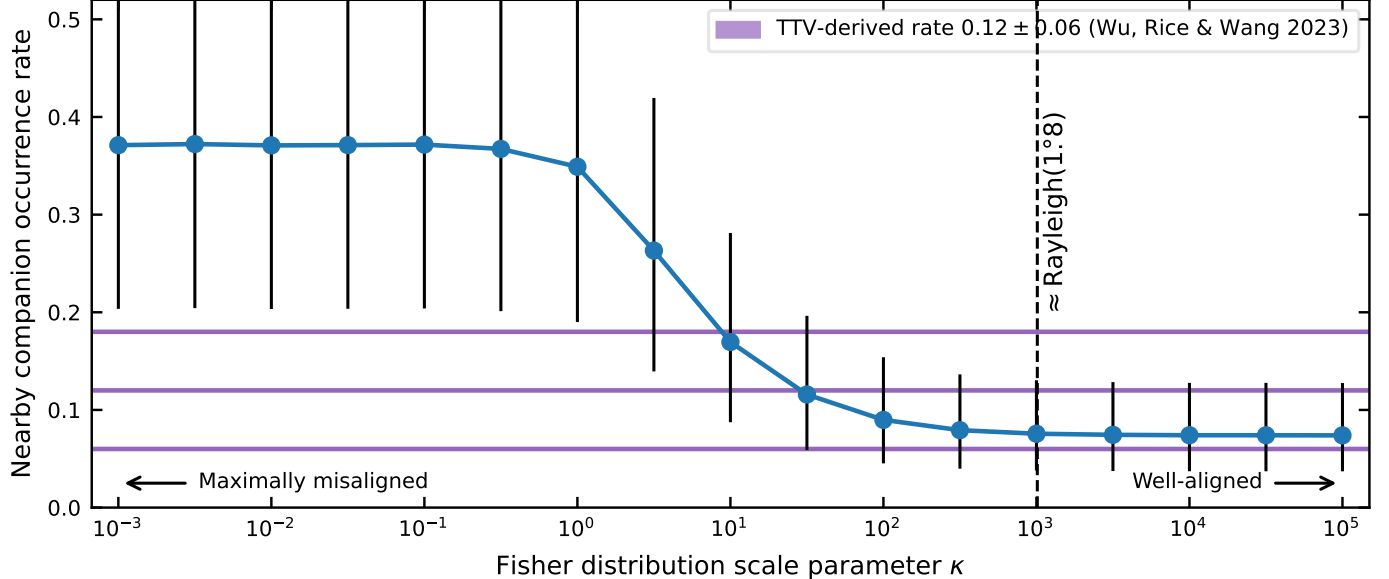


Figure 7. Occurrence rate of nearby companions ($0.25 \text{ d} \leq P < 10 \text{ d}$, $1 \leq R_p/R_\oplus < 4$) to hot jupiters as a function of their orbital alignment, parameterized as the scale parameter κ of a Fisher distribution prior on their mutual inclination. The posterior of each occurrence rate is a beta distribution, and we take the median and 90% interval as the marks and error bars shown. The vertical line ($\kappa \approx 10^3$) corresponds to the Rayleigh(1.8°) distribution, which was used as the mutual inclination prior to derive our main occurrence rate result of $(7.6^{+5.5}_{-3.8})\%$. For comparison, we shaded the $(12 \pm 6)\%$ credible interval of a similar occurrence rate derived from transit-timing variations of hot jupiters from the *Kepler* mission by D.-H. Wu et al. (2023). While their occurrence rate is not directly comparable to ours, reconciling the two different detection methods appears to rule out the case of maximal misalignment between hot jupiters and their nearby companions.

the observational completeness of nearby companions, because they must transit in order to be detected in our search. Having explored how the degree of alignment between hot jupiters and their nearby companions affects the calculated occurrence rate in subsection 5.5, we now compare our result to occurrence rates derived from transit-timing variations (TTVs) of hot jupiters, which can detect non-transiting companions by their gravitational influence on a hot jupiter’s orbit..

After a comprehensive search for TTVs among all hot jupiters observed by *Kepler*, Wu, Rice, & Wang (2023) found two TTV signals among 50 hot jupiters in their sample, implying an occurrence rate of $(12 \pm 6)\%$ for nearby companions to hot jupiters, where “nearby” is defined as having a period ratio $\approx 1.5\text{--}4$. Their result is highlighted in Figure 7. Although their result is not directly comparable to ours due to difference in the assumption of priors for the underlying distribution of nearby companions and the different detection characteristics of TTV- and transit-based methods, reconciling the rates derived from the two methods appears to be incompatible with the case of maximal misalignment between hot jupiters and their nearby companions (i.e. $\kappa \ll 1$). This would rule out unusual formation scenarios that result in the hot jupiter and its companion being in nearly perpendicular orbits, as would be the case suggested by K. Batygin et al. (2016).

A more careful comparison between the TTV- and transit-based methods would require a joint search for TTVs and tran-

sits among a complete sample of well-characterized *Kepler* and *TESS* hot jupiters. As a first step towards this process, we note that Z. Zhang et al. (2024) have performed a TTV search among 260 hot jupiters from *TESS* hot jupiters, constraining the upper mass limit for potential companions to be several M_J . A future work could combine and extend the results from D.-H. Wu et al. (2023), Z. Zhang et al. (2024), and this work and invert the statistical framework used to derive occurrence rates to instead constrain the underlying distribution of mutual inclinations in systems hosting hot jupiters with nearby companions.

6.3. Do hot jupiter inner companions have a small preferential misalignment?

We can also learn about the mutual inclination distribution of the hot jupiters and their close neighbors by studying the impact parameter distributions of the systems in our sample. We note that among the nine hot jupiters with inner companions, four of them (TOI-1408, TOI-5143, TOI-2494, and TOI-1130) have grazing transits. Whether a single transiting planet is grazing depends only on the geometry of an observer viewing a randomly oriented orbital plane. In a system of two transiting planets, however, the probability of either of the planets grazing also depends on their mutual inclination. If the two planets are perfectly aligned ($\psi = 0$), then the probability of finding a grazing planet is independent from the existence of the other transiting planet. But if the two planets are slightly misaligned, then the probability

of finding one of the planets grazing given the presence of another transiting planet in the same system is boosted from what one might expect by random alignment. Here, we investigate whether finding four out of nine grazing hot jupiters is more than what chance alignment can explain.

In order to calculate the grazing probability, we took the planet-to-stellar radius ratio of the i th hot jupiter $k_i = R_{p,i}/R_{\star,i}$ and calculated the grazing probability p_i as

$$p_i = \frac{2k_i}{1 + k_i}. \quad (18)$$

Then, we average the grazing probability and used the average $p = (\sum_{i=1}^9 p_i)/9$ as the parameter of a binomial distribution with the PDF

$$f_{\text{binom}}(k; n, p) = \binom{n}{k} p^k (1 - p)^{n-k}, \quad (19)$$

where $n = 9$. Since the four planets are grazing, their radii are not known precisely, so we assume $R_p = 1 R_J$. This gives an average grazing probability $p = 0.19$, which implies that the probability of having 4 or more grazing planets due to random viewing geometry to be

$$\Pr(\geq 4 \text{ grazing}) = \sum_{k=4}^9 f_{\text{binom}}(k; 9, 0.19) \approx 0.075. \quad (20)$$

This tantalizing statistical hint merits more investigation as we detect more samples in the future. If hot jupiters with transiting inner companions are more likely to be grazing than we would expect from the random orientation of the viewing geometry alone, as would be the case for solitary hot jupiters without nearby companions, then there may be a systematic small misalignment between these hot jupiters and their inner companions. This misalignment could be the remnant dynamic signature of past migration.

6.4. hot jupiters with inner companions also have cold outer companions

We can also investigate the systems with close companions and study their architectures beyond short-period transiting system. Although transits are an effective way of finding additional planets in hot jupiter systems, they may not give us the full picture of the architecture of these systems as transit probability falls off for longer orbital periods. Indeed, using up to 30 yr of RV measurements from the California Legacy Survey, (J. K. Zink & A. W. Howard 2023) found that virtually all hot jupiters have at least one more “cold” companion at much greater orbital periods. Since the very presence of these cold companions likely caused the hot jupiters to migrate inward after disk dispersal, it would be instructive to look for cold companions in hot jupiter systems with nearby companions to see whether they differ from the hot jupiter population at large. Here, we assemble evidence from the literature for cold outer companions.

1. **WASP-47.** M. Neveu-VanMalle et al. (2016) found a cold companion WASP-47 c with orbital period $P = (588.8 \pm 2.0)$ d and minimum mass $M_p \sin i = (398.9 \pm 9.1) M_{\oplus}$ (E. M. Bryant & D. Bayliss 2022). Additionally, WASP-47 d is a nearby outer companion (J. C. Becker et al. 2015).
2. **WASP-132.** Planet d is detected by RV with $P = (1811.8^{+42.6}_{-44.4})$ d, $M_p \sin i = (5.29^{+0.48}_{-0.46}) M_J$ (N. Grieves et al. 2025). There is an additional linear trend in the RV (with a baseline of ≈ 9 yr implying $P \gtrsim 18$ yr) that may be a brown dwarf, in line with evidence for excess astrometric uncertainty in *Gaia* DR2 and DR3.
3. **TOI-1130.** There is an additional linear trend implying $P \gtrsim 160$ d (L. Borsato et al. 2024).
4. **TOI-1408.** There is an additional nonlinear trend implying $P \approx 2530$ d, $M \approx (14.6 \pm 0.3) M_J$ (J. Korth et al. 2024).

In addition, TOI-2000 showed planet-sized RV signals at ≈ 17 d and ≈ 90 d not explained by spectroscopic stellar activity indicators or photometric variations (L. Sha et al. 2023), although the RV baseline was too short to draw any conclusions at the time. Since then, the High Accuracy Radial velocity Planet Searcher (HARPS) spectrograph at the ESO La Silla 3.6 m telescope has made 39 additional RV measurements from 2023 December to 2024 March,³⁰ which showed an overall offset from the RVs three years prior in 2021 at the 20 m s^{-1} level, although it is too early to say whether this offset is due to long-term stellar activity or an additional long-period planet.

Given that these systems are newly characterized and lack long-term RV monitoring, it is quite possible that there are cold outer companions in the remaining systems whose signals are hiding in plain sight, which would imply that hot jupiters with nearby companions seem to also have cold companions comparable to the rate for other hot jupiters in general estimated by (J. K. Zink & A. W. Howard 2023). The presence of outer companions is believed to be a viable way to kickstart HEM, but if hot jupiters with nearby companions, which presumably did not undergo HEM, also have similar (or even greater) prevalence of outer companions, then the link between outer companions and HEM would be more complicated than it currently appears; namely, the mere presence of a cold companion is not sufficient to trigger HEM in producing an hot jupiter. Continued long-term RV monitoring of these systems can potentially reveal this potential tension by comparing the mass and eccentricity of these suspected cold companions to the distribution of other hot jupiters’ cold companions.

³⁰ ESO program 112.25WB, PI: Chelsea X. Huang.

6.5. Implications on formation theories

In summary, we find that about $(7.6^{+5.5}_{-3.8})\%$ of all hot jupiters have closely orbiting companion planets, that the mutual inclination of these planets is small, but nonzero and probably larger than the mutual inclination of small planet systems, and that the frequency of long-period outer companions seems similar to hot jupiters without close companion planets. We draw the following conclusions about the formation of hot jupiters.

1. At least $(7.6^{+5.5}_{-3.8})\%$ of hot jupiters (e.g. the ones with nearby companions) must not form via high-eccentricity migration, which would almost certainly disrupt any nearby planetary companions. Moreover, the likely low mutual inclinations between hot jupiters and their close companions also suggests relatively quiescent formation scenarios.
2. Moreover, since $(7.6^{+5.5}_{-3.8})\%$ is a strict lower limit on the fraction of systems that formed via dynamically quiescent mechanisms, the true fraction of hot jupiters that form in this way could be larger. For example, simulations of hot jupiters with nearby companions that formed via disk migration indicate that only about 1/3 of such close companions survive for long timescales (D.-H. Wu & Y. He 2023). This means that our result that $(7.6^{+5.5}_{-3.8})\%$ of hot jupiters have close companions is consistent with a larger fraction ($\approx 20\%$) of hot jupiter systems forming via disk migration.

Going forward, more detailed measurements and studies of the architectures of these systems, including the occurrence rate of specifically ultra-short-period planets (S. Wang et al. 2025), stellar obliquities and mutual inclinations (Y. He et al. 2024), and long-term RV surveys to measure the frequency of long-period massive planets (J. K. Zink & A. W. Howard 2023) will make it possible to estimate the relative importance of the different hot jupiter formation channels.

7. CONCLUSIONS

Using five years of *TESS* data, we have performed the most comprehensive search for nearby transiting companion planets to hot jupiters to date. After accounting for observational completeness and pipeline detection efficiency, we arrived at an intrinsic occurrence rate of $(7.6^{+5.5}_{-3.8})\%$ for nearby companions to hot jupiters. This result is highly sensitive to the assumption for the mutual inclination distribution between the hot jupiters and their companions, and we instead have $(37^{+19}_{-17})\%$ for the case of maximal misalignment and $(7.4^{+5.4}_{-3.7})\%$ for the case of perfect alignment. Comparing our rate based on transit detections to that based on TTV detections appears to disfavor the case of maximal misalignment,

but there may nevertheless be a preference for small misalignment as there is a hint that more hot jupiters with nearby companions are grazing than can be explained by random viewing geometry. A review of RVs in the literature reveals that about half of the known hot jupiters with nearby companions either have or are suspected to have cold companions, raising questions about the role cold companions play in triggering the formation of hot jupiters via HEM. A future comprehensive search for nearby companions with transits, TTVs, and RVs may elucidate the underlying mutual inclination and provide a key constraint on the outcome of hot jupiter formation. The picture is emerging that these nearby companions to hot jupiters, while a relatively uncommon outcome of hot jupiter formation, provide a key constraint on the relative frequency of each formation channel.

ACKNOWLEDGMENTS

We thank Joshua N. Winn for suggestions that led to our implementation of subsection 6.1.

Funding for the TESS mission is provided by NASA's Science Mission Directorate. We acknowledge the use of public TESS data from pipelines at the TESS Science Office and at the TESS Science Processing Operations Center. This research has made use of the Exoplanet Follow-up Observation Program website (ExoFOP; NExScI 2022), which is operated by the California Institute of Technology, under contract with the National Aeronautics and Space Administration under the Exoplanet Exploration Program. This paper includes data collected by the TESS mission that are publicly available from the Mikulski Archive for Space Telescopes (MAST).

This work makes use of observations from the LCOGT network. Part of the LCOGT telescope time was granted by NOIRLab through the Mid-Scale Innovations Program (MSIP). MSIP is funded by NSF. This paper is based on observations made with the Las Cumbres Observatory's education network telescopes that were upgraded through generous support from the Gordon and Betty Moore Foundation. This paper is based on observations made with the MuSCAT instruments, developed by the Astrobiology Center (ABC) in Japan, the University of Tokyo, and Las Cumbres Observatory (LCOGT). MuSCAT3 was developed with financial support by JSPS KAKENHI (JP18H05439) and JST PRESTO (JPMJPR1775), and is located at the Faulkes Telescope North on Maui, HI (USA), operated by LCOGT. MuSCAT4 was developed with financial support provided by the Heising-Simons Foundation (grant 2022-3611), JST grant number JP-MJCR1761, and the ABC in Japan, and is located at the Faulkes Telescope South at Siding Spring Observatory (Australia), operated by LCOGT.

Funding for KB was provided by the European Union (ERC AdG SUBSTELLAR, GA 101054354).

AB acknowledges the support of M.V. Lomonosov Moscow State University Program of Development.

KAC acknowledges support from the TESS mission via subaward s3449 from MIT.

TG acknowledges that ASTEP benefited from the support of the French and Italian polar agencies IPEV and PNRA in the framework of the Concordia station program and from OCA, INSU, Idex UCAJEDI (ANR-15-IDEX-01), ESA through the Science Faculty of the European Space Research and Technology Centre (ESTEC), the European Research Council (ERC) under the European Union's Horizon 2020 research and innovation program (grant agreement n° 803193/BEBOP), and from the Science and Technology Facilities Council (STFC; grant n° ST/S00193X/1, ST/W002582/1, and ST/Y001710/1).

FM acknowledges the financial support from the Agencia Estatal de Investigación del Ministerio de Ciencia, Innovación y Universidades (MCIU/AEI) through grant PID2023-152906NA-I00.

This work is partly supported by JSPS KAKENHI Grant Numbers JP24H00017, JP24K00689, JP24H00248, JP24K17082, JP24K17083, JSPS Grant-in-Aid for JSPS Fellows Grant Numbers JP24KJ0241, JP25KJ0091, and JSPS Bilateral Program Number JPJSBP120249910. This article is based on observations made with the MuSCAT2 instrument, developed by ABC, at Telescopio Carlos Sánchez operated on

the island of Tenerife by the IAC in the Spanish Observatorio del Teide. This paper is based on observations made with the MuSCAT instruments, developed by the Astrobiology Center (ABC) in Japan, the University of Tokyo, and Las Cumbres Observatory (LCOGT). MuSCAT3 was developed with financial support by JSPS KAKENHI (JP18H05439) and JST PRESTO (JPMJPR1775), and is located at the Faulkes Telescope North on Maui, HI (USA), operated by LCOGT. MuSCAT4 was developed with financial support provided by the Heising-Simons Foundation (grant 2022-3611), JST grant number JPMJCR1761, and the ABC in Japan, and is located at the Faulkes Telescope South at Siding Spring Observatory (Australia), operated by LCOGT.

EP acknowledge financial support from the Agencia Estatal de Investigación of the Ministerio de Ciencia e Innovación MCIN/AEI/10.13039/501100011033 and the ERDF “A way of making Europe” through project PID2021-125627OB-C32, and from the Centre of Excellence “Severo Ochoa” award to the Instituto de Astrofísica de Canarias.

Software: Astropy (Astropy Collaboration et al. 2013, 2018, 2022), MIT Quick Look Pipeline (QLP) (C. X. Huang 2020; C. X. Huang et al. 2020b,c; M. Kunimoto et al. 2021, 2022b), giants (N. Saunders et al. 2022), tess-diffImage, Pandas,

Facilities: *Gaia, TESS*

REFERENCES

Agresti, A., & Coull, B. 1998, *The American Statistician*, 52, 119, doi: [10.2307/2685469](https://doi.org/10.2307/2685469)

Astropy Collaboration, Robitaille, T. P., Tollerud, E. J., et al. 2013, *A&A*, 558, A33, doi: [10.1051/0004-6361/201322068](https://doi.org/10.1051/0004-6361/201322068)

Astropy Collaboration, Price-Whelan, A. M., Sipőcz, B. M., et al. 2018, *AJ*, 156, 123, doi: [10.3847/1538-3881/aabc4f](https://doi.org/10.3847/1538-3881/aabc4f)

Astropy Collaboration, Price-Whelan, A. M., Lim, P. L., et al. 2022, *ApJ*, 935, 167, doi: [10.3847/1538-4357/ac7c74](https://doi.org/10.3847/1538-4357/ac7c74)

Batygin, K., Bodenheimer, P. H., & Laughlin, G. P. 2016, *ApJ*, 829, 114, doi: [10.3847/0004-637X/829/2/114](https://doi.org/10.3847/0004-637X/829/2/114)

Becker, J. C., Vanderburg, A., Adams, F. C., Khain, T., & Bryan, M. 2017, *AJ*, 154, 230, doi: [10.3847/1538-3881/aa9176](https://doi.org/10.3847/1538-3881/aa9176)

Becker, J. C., Vanderburg, A., Adams, F. C., Rappaport, S. A., & Schwengeler, H. M. 2015, *ApJL*, 812, L18, doi: [10.1088/2041-8205/812/2/L18](https://doi.org/10.1088/2041-8205/812/2/L18)

Beleznay, M., & Kunimoto, M. 2022, *MNRAS*, 516, 75, doi: [10.1093/mnras/stac2179](https://doi.org/10.1093/mnras/stac2179)

Borsato, L., Degen, D., Leleu, A., et al. 2024, *A&A*, 689, A52, doi: [10.1051/0004-6361/202450974](https://doi.org/10.1051/0004-6361/202450974)

Bryant, E. M., & Bayliss, D. 2022, *AJ*, 163, 197, doi: [10.3847/1538-3881/ac58ff](https://doi.org/10.3847/1538-3881/ac58ff)

Burke, C. J., Christiansen, J. L., Mullally, F., et al. 2015, *ApJ*, 809, 8, doi: [10.1088/0004-637X/809/1/8](https://doi.org/10.1088/0004-637X/809/1/8)

Cañas, C. I., Wang, S., Mahadevan, S., et al. 2019, *ApJL*, 870, L17, doi: [10.3847/2041-8213/aafa1e](https://doi.org/10.3847/2041-8213/aafa1e)

Choi, J., Dotter, A., Conroy, C., et al. 2016, *ApJ*, 823, 102, doi: [10.3847/0004-637X/823/2/102](https://doi.org/10.3847/0004-637X/823/2/102)

Christiansen, J. L., Clarke, B. D., Burke, C. J., et al. 2015, *ApJ*, 810, 95, doi: [10.1088/0004-637X/810/2/95](https://doi.org/10.1088/0004-637X/810/2/95)

Coughlin, J. L., Thompson, S. E., Bryson, S. T., et al. 2014, *AJ*, 147, 119, doi: [10.1088/0004-6256/147/5/119](https://doi.org/10.1088/0004-6256/147/5/119)

Dotter, A. 2016, *ApJS*, 222, 8, doi: [10.3847/0067-0049/222/1/8](https://doi.org/10.3847/0067-0049/222/1/8)

Fabrycky, D. C., & Winn, J. N. 2009, *ApJ*, 696, 1230, doi: [10.1088/0004-637X/696/2/1230](https://doi.org/10.1088/0004-637X/696/2/1230)

Fabrycky, D. C., Lissauer, J. J., Ragozzine, D., et al. 2014, *ApJ*, 790, 146, doi: [10.1088/0004-637X/790/2/146](https://doi.org/10.1088/0004-637X/790/2/146)

Fausnaugh, M. M., Burke, C. J., Ricker, G. R., & Vanderspek, R. 2020, *Research Notes of the American Astronomical Society*, 4, 251, doi: [10.3847/2515-5172/abd63a](https://doi.org/10.3847/2515-5172/abd63a)

Grieves, N., Bouchy, F., Armstrong, D. J., et al. 2025, *A&A*, 693, A144, doi: [10.1051/0004-6361/202348177](https://doi.org/10.1051/0004-6361/202348177)

Guerrero, N. M., Seager, S., Huang, C. X., et al. 2021, *ApJS*, 254, 39, doi: [10.3847/1538-4365/abefe1](https://doi.org/10.3847/1538-4365/abefe1)

Hartman, J. D., & Bakos, G. A. 2016, *A&C*, 17, 1, doi: [10.1016/j.ascom.2016.05.006](https://doi.org/10.1016/j.ascom.2016.05.006)

He, Y., Wu, D.-H., & Jin, S. 2024, *MNRAS*, 530, 3934, doi: [10.1093/mnras/stae1076](https://doi.org/10.1093/mnras/stae1076)

Hoffman, J. 2022, cuvarbase: fast period finding utilities for GPUs, *Astrophysics Source Code Library*, record ascl:2210.030

Hord, B. J., Colón, K. D., Kostov, V., et al. 2021, *AJ*, 162, 263, doi: [10.3847/1538-3881/ac2602](https://doi.org/10.3847/1538-3881/ac2602)

Hord, B. J., Colón, K. D., Berger, T. A., et al. 2022, *AJ*, 164, 13, doi: [10.3847/1538-3881/ac6f57](https://doi.org/10.3847/1538-3881/ac6f57)

Huang, C., Wu, Y., & Triaud, A. H. M. J. 2016, *ApJ*, 825, 98, doi: [10.3847/0004-637X/825/2/98](https://doi.org/10.3847/0004-637X/825/2/98)

Huang, C. X. 2020, TESS Lightcurves From The MIT Quick-Look Pipeline, *STScI/MAST*, doi: [10.17909/T9-R086-E880](https://doi.org/10.17909/T9-R086-E880)

Huang, C. X., Quinn, S. N., Vanderburg, A., et al. 2020a, *ApJL*, 892, L7, doi: [10.3847/2041-8213/ab7302](https://doi.org/10.3847/2041-8213/ab7302)

Huang, C. X., Vanderburg, A., Pál, A., et al. 2020b, *Research Notes of the American Astronomical Society*, 4, 204, doi: [10.3847/2515-5172/abca2e](https://doi.org/10.3847/2515-5172/abca2e)

Huang, C. X., Vanderburg, A., Pál, A., et al. 2020c, *Research Notes of the American Astronomical Society*, 4, 206, doi: [10.3847/2515-5172/abca2d](https://doi.org/10.3847/2515-5172/abca2d)

Korth, J., Chaturvedi, P., Parviainen, H., et al. 2024, *ApJL*, 971, L28, doi: [10.3847/2041-8213/ad65fd](https://doi.org/10.3847/2041-8213/ad65fd)

Kovács, G., Zucker, S., & Mazeh, T. 2002, *A&A*, 391, 369, doi: [10.1051/0004-6361:20020802](https://doi.org/10.1051/0004-6361:20020802)

Kunimoto, M., Tey, E., Fong, W., et al. 2023, *Research Notes of the American Astronomical Society*, 7, 28, doi: [10.3847/2515-5172/acbc13](https://doi.org/10.3847/2515-5172/acbc13)

Kunimoto, M., Tey, E., Fong, W., Hesse, K., & Shporer, A. 2022a, *Research Notes of the American Astronomical Society*, 6, 235, doi: [10.3847/2515-5172/aca157](https://doi.org/10.3847/2515-5172/aca157)

Kunimoto, M., Tey, E., Fong, W., et al. 2022b, *Research Notes of the American Astronomical Society*, 6, 236, doi: [10.3847/2515-5172/aca158](https://doi.org/10.3847/2515-5172/aca158)

Kunimoto, M., Huang, C., Tey, E., et al. 2021, *Research Notes of the American Astronomical Society*, 5, 234, doi: [10.3847/2515-5172/ac2ef0](https://doi.org/10.3847/2515-5172/ac2ef0)

Latham, D. W., Rowe, J. F., Quinn, S. N., et al. 2011, *ApJL*, 732, L24, doi: [10.1088/2041-8205/732/2/L24](https://doi.org/10.1088/2041-8205/732/2/L24)

Lin, D. N. C., Bodenheimer, P., & Richardson, D. C. 1996, *Nature*, 380, 606, doi: [10.1038/380606a0](https://doi.org/10.1038/380606a0)

Maciejewski, G., Golonka, J., Łoboda, W., et al. 2023, *MNRAS*, 525, L43, doi: [10.1093/mnrasl/slad078](https://doi.org/10.1093/mnrasl/slad078)

Mayor, M., & Queloz, D. 1995, *Nature*, 378, 355, doi: [10.1038/378355a0](https://doi.org/10.1038/378355a0)

McKee, B. J., Montet, B. T., Yee, S. W., et al. 2025, *ApJ*, 981, 106, doi: [10.3847/1538-4357/adac63](https://doi.org/10.3847/1538-4357/adac63)

McLaughlin, D. B. 1924, *ApJ*, 60, 22, doi: [10.1086/142826](https://doi.org/10.1086/142826)

Miller-Ricci, E., Rowe, J. F., Sasselov, D., et al. 2008, *ApJ*, 682, 593, doi: [10.1086/587634](https://doi.org/10.1086/587634)

Morton, T. D. 2015, isochrones: Stellar model grid package,, *Astrophysics Source Code Library*, record ascl:1503.010

Neveu-VanMalle, M., Queloz, D., Anderson, D. R., et al. 2016, *A&A*, 586, A93, doi: [10.1051/0004-6361/201526965](https://doi.org/10.1051/0004-6361/201526965)

NExScI. 2022, Exoplanet Follow-up Observing Program Web Service, *IPAC*, doi: [10.26134/EXOFOPS](https://doi.org/10.26134/EXOFOPS)

Pollack, J. B., Hubickyj, O., Bodenheimer, P., et al. 1996, *Icarus*, 124, 62, doi: [10.1006/icar.1996.0190](https://doi.org/10.1006/icar.1996.0190)

Rasio, F. A., & Ford, E. B. 1996, *Science*, 274, 954, doi: [10.1126/science.274.5289.954](https://doi.org/10.1126/science.274.5289.954)

Rodriguez, J. E., Quinn, S. N., Zhou, G., et al. 2021, *AJ*, 161, 194, doi: [10.3847/1538-3881/abe38a](https://doi.org/10.3847/1538-3881/abe38a)

Rodriguez, J. E., Quinn, S. N., Vanderburg, A., et al. 2023, *MNRAS*, 521, 2765, doi: [10.1093/mnras/stad595](https://doi.org/10.1093/mnras/stad595)

Rossiter, R. A. 1924, *ApJ*, 60, 15, doi: [10.1086/142825](https://doi.org/10.1086/142825)

Saunders, N., Grunblatt, S. K., Huber, D., et al. 2022, *AJ*, 163, 53, doi: [10.3847/1538-3881/ac38a1](https://doi.org/10.3847/1538-3881/ac38a1)

Schulte, J., Rodriguez, J. E., Bieryla, A., et al. 2024, *AJ*, 168, 32, doi: [10.3847/1538-3881/ad4a57](https://doi.org/10.3847/1538-3881/ad4a57)

Sha, L., Vanderburg, A. M., Huang, C. X., et al. 2023, *MNRAS*, 524, 1113, doi: [10.1093/mnras/stad1666](https://doi.org/10.1093/mnras/stad1666)

Shallue, C. J., & Vanderburg, A. 2018, *AJ*, 155, 94, doi: [10.3847/1538-3881/aa9e09](https://doi.org/10.3847/1538-3881/aa9e09)

Stassun, K. G., Oelkers, R. J., Pepper, J., et al. 2018, *AJ*, 156, 102, doi: [10.3847/1538-3881/aad050](https://doi.org/10.3847/1538-3881/aad050)

Stassun, K. G., Oelkers, R. J., Paegert, M., et al. 2019, *AJ*, 158, 138, doi: [10.3847/1538-3881/ab3467](https://doi.org/10.3847/1538-3881/ab3467)

Steffen, J. H., Ragozzine, D., Fabrycky, D. C., et al. 2012, *Proceedings of the National Academy of Science*, 109, 7982, doi: [10.1073/pnas.1120970109](https://doi.org/10.1073/pnas.1120970109)

Thompson, S. E., Coughlin, J. L., Hoffman, K., et al. 2018a, *ApJS*, 235, 38, doi: [10.3847/1538-4365/aab4f9](https://doi.org/10.3847/1538-4365/aab4f9)

Thompson, S. E., Coughlin, J. L., Hoffman, K., et al. 2018b, *ApJS*, 235, 38, doi: [10.3847/1538-4365/aab4f9](https://doi.org/10.3847/1538-4365/aab4f9)

Vanderburg, A., & Johnson, J. A. 2014, *PASP*, 126, 948, doi: [10.1086/678764](https://doi.org/10.1086/678764)

Vanderburg, A., Latham, D. W., Buchhave, L. A., et al. 2016, *ApJS*, 222, 14, doi: [10.3847/0067-0049/222/1/14](https://doi.org/10.3847/0067-0049/222/1/14)

Vanderburg, A., Huang, C. X., Rodriguez, J. E., et al. 2019, *ApJL*, 881, L19, doi: [10.3847/2041-8213/ab322d](https://doi.org/10.3847/2041-8213/ab322d)

Wang, S., Pan, M., Dong, Y., Zhao, G., & Ji, J. 2025, *ApJL*, 982, L15, doi: [10.3847/2041-8213/adbae6](https://doi.org/10.3847/2041-8213/adbae6)

Wright, J. T., Marcy, G. W., Howard, A. W., et al. 2012, *ApJ*, 753, 160, doi: [10.1088/0004-637X/753/2/160](https://doi.org/10.1088/0004-637X/753/2/160)

Wu, D.-H., & He, Y. 2023, *AJ*, 166, 267, doi: [10.3847/1538-3881/ad09b0](https://doi.org/10.3847/1538-3881/ad09b0)

Wu, D.-H., Rice, M., & Wang, S. 2023, *AJ*, 165, 171, doi: [10.3847/1538-3881/acbf3f](https://doi.org/10.3847/1538-3881/acbf3f)

Yee, S. W., & Winn, J. N. 2023, *ApJL*, 949, L21,
doi: [10.3847/2041-8213/acd552](https://doi.org/10.3847/2041-8213/acd552)

Yee, S. W., Winn, J. N., & Hartman, J. D. 2021, *AJ*, 162, 240,
doi: [10.3847/1538-3881/ac2958](https://doi.org/10.3847/1538-3881/ac2958)

Yee, S. W., Winn, J. N., Hartman, J. D., et al. 2022, *AJ*, 164, 70,
doi: [10.3847/1538-3881/ac73ff](https://doi.org/10.3847/1538-3881/ac73ff)

Yee, S. W., Winn, J. N., Hartman, J. D., et al. 2023, *ApJS*, 265, 1,
doi: [10.3847/1538-4365/aca286](https://doi.org/10.3847/1538-4365/aca286)

Zhang, Z., Wang, W., Ma, X., et al. 2024, *ApJS*, 275, 32,
doi: [10.3847/1538-4365/ad89a6](https://doi.org/10.3847/1538-4365/ad89a6)

Zhou, G., Huang, C. X., Bakos, G. Á., et al. 2019, *AJ*, 158, 141,
doi: [10.3847/1538-3881/ab36b5](https://doi.org/10.3847/1538-3881/ab36b5)

Zhu, W., Dai, F., & Masuda, K. 2018, *Research Notes of the American Astronomical Society*, 2, 160,
doi: [10.3847/2515-5172/aade53](https://doi.org/10.3847/2515-5172/aade53)

Zink, J. K., & Howard, A. W. 2023, *ApJL*, 956, L29,
doi: [10.3847/2041-8213/acfdab](https://doi.org/10.3847/2041-8213/acfdab)

All Authors and Affiliations

LIZHOU SHA ¹ ANDREW M. VANDERBURG ² CHELSEA X. HUANG ³ SAMUEL CHRISTIAN ⁴ NICHOLAS SAUNDERS ^{5,6}
KHALID BARKAOUI ^{7,8,9} ALEXANDER BELINSKI ^{10,11} SERGE BERGERON ^{12,13} ALLYSON BIERYLA ² KAREN A. COLLINS ²
GIUSEPPE CONZO ¹⁴ AKIHIKO FUKUI ^{15,7} TRISTAN GUILLOT ¹⁶ KAI IKUTA ¹⁷ DAVID W. LATHAM ² JEROME P. DE LEON ¹⁵
BOB MASSEY ¹³ GABRIEL MURAWSKI ¹⁸ FELIPE MURGAS ^{7,19} NORIO NARITA ^{15,20,7} MOHAMMAD ODEH ²¹ ENRIC PALLE ^{7,19}
RICHARD P. SCHWARZ ² GREGOR SRDOC,²² CHRIS STOCKDALE ²³ IAN A. WAITE ³ AND FRANCIS P. WILKIN ²⁴

¹*Department of Astrophysical Sciences, Princeton University, 4 Ivy Ln, Princeton, NJ 08540 USA*

²*Center for Astrophysics | Harvard & Smithsonian, 60 Garden Street, Cambridge, MA 02138, USA*

³*Centre for Astrophysics, University of Southern Queensland, Toowoomba, Queensland 4350, Australia*

⁴*Department of Physics and Kavli Institute for Astrophysics and Space Research, Massachusetts Institute of Technology, 77 Massachusetts Ave, Cambridge, MA 02139, USA*

⁵*Department of Astronomy, Yale University, New Haven, CT 06511, USA*

⁶*Institute for Astronomy, University of Hawaii at Mānoa, 2680 Woodlawn Drive, Honolulu, HI 96822, USA*

⁷*Instituto de Astrofísica de Canarias (IAC), E-38200 La Laguna, Tenerife, Spain*

⁸*Astrobiology Research Unit, Université de Liège, Allée du 6 Août 19C, B-4000 Liège, Belgium*

⁹*Department of Earth, Atmospheric and Planetary Science, Massachusetts Institute of Technology, 77 Massachusetts Ave, Cambridge, MA 02139, USA*

¹⁰*Sternberg Astronomical Institute, Lomonosov Moscow State University, Universitetskii prospekt, 13, Moscow 119992, Russia*

¹¹*Faculty of Physics, Moscow State University, 1 bldg. 2, Leninskie Gory, Moscow 119991, Russia*

¹²*American Public University*

¹³*American Association of Variable Star Observers, 185 Alewife Brook Pkwy Ste 410, Cambridge, MA 02138, USA*

¹⁴*Gruppo Astrofili Palidoro, Italy*

¹⁵*Komaba Institute for Science, The University of Tokyo, 3-8-1 Komaba, Meguro, Tokyo 153-8902, Japan*

¹⁶*Observatoire de la Côte d'Azur, Université Côte d'Azur, CNRS, Laboratoire Lagrange, Bd de l'Observatoire, CS 34229, 06304 Nice cedex 4, France*

¹⁷*Department of Social Data Science, Hitotsubashi University, 2-1 Naka, Kunitachi, Tokyo 186-8601, Japan*

¹⁸*Gabriel Murawski Private Observatory (SOTES)*

¹⁹*Departamento de Astrofísica, Universidad de La Laguna (ULL), E-38206 La Laguna, Tenerife, Spain*

²⁰*Astrobiology Center, 2-21-1 Osawa, Mitaka, Tokyo 181-8588, Japan*

²¹*International Astronomical Center, 45015, Abu Dhabi, United Arab Emirates*

²²*Kotizarovci Observatory, Sarsoni 90, 51216 Viskovo, Croatia*

²³*Hazelwood Observatory, Australia*

²⁴*Union College, Schenectady, NY 12308 USA*